Calvin University

Calvin Digital Commons

4-20-2003

An extended burst tail from SGR 1900+14 with a thermal x-ray spectrum

Geoffrey T. Lenters
Calvin University

Peter M. Woods
NASA Marshall Space Flight Center

Johnathan E. Goupell
Hope College

Chryssa Kouveliotou
NASA Marshall Space Flight Center

Follow this and additional works at: https://digitalcommons.calvin.edu/calvin_facultypubs

Part of the Astrophysics and Astronomy Commons

Recommended Citation

AN EXTENDED BURST TAIL FROM SGR 1900+14 WITH A THERMAL X-RAY SPECTRUM

Geoffrey T. Lenters,[1] Peter M. Woods,[2,3] Johnathan E. Goupell,[4] Chryssa Kouveliotou,[2,3]
Ersin Göğüş,[2,3] Kevin Hurley,[5] Dmitry Frederiks,[6] Sergey Golenetskii,[6] and Jean Swank[7]

ABSTRACT

The soft gamma repeater SGR 1900+14 entered a new phase of activity in 2001 April initiated by the intermediate flare recorded on April 18. Ten days following this flare, we discovered an abrupt increase in the source flux between consecutive *Rossi X-Ray Timing Explorer* (*RXTE*) orbits. This X-ray flux excess decayed over the next several minutes and was subsequently linked to a high fluence burst from SGR 1900+14 recorded by other spacecraft (*Ulysses* and *Wind*/Konus) while the SGR was Earth-occulted for *RXTE*. We present here spectral and temporal analysis of both the burst of April 28 and the long X-ray tail following it. We find strong evidence of an exclusively thermal X-ray tail in this event and bring this evidence to bear on other bursts and flares from SGR 1900+14 that have shown extended X-ray excesses (e.g., 1998 August 29). We include in this comparison a discussion of the physical origins of SGR bursts and extended X-ray tails.

Subject headings: stars: individual (SGR 1900+14) — stars: neutron — X-rays: bursts

1. INTRODUCTION

Soft gamma repeaters (SGRs) are a small class of astrophysical objects (currently four confirmed sources and one candidate source [Hurley 2000]) discovered by their emission of bright bursts of soft gamma rays (with peak luminosities ranging between 10^{38} and 10^{44} ergs s^{-1}). The SGR quiescent counterparts have X-ray luminosities of 10^{34} ergs s^{-1}, and their energy spectra are generally well fitted with a power-law model (index of ~ -2.2) attenuated by interstellar absorption; however, SGR 1900+14 has shown clear evidence of an additional blackbody component with $kT \sim 0.5$ keV (Woods et al. 1999a, 2001; Kouveliotou et al. 2001). Coherent pulsations have been detected in the persistent emission of two sources (SGR 1806−20 at 7.5 s [Kouveliotou et al. 1998] and SGR 1900+14 at 5.2 s [Hurley et al. 1999b]) with a spin-down rate of $\sim 10^{-10}$ s s^{-1} (Kouveliotou et al. 1998, 1999). The Galactic SGRs (three) are located very close to the plane of the Galaxy, indicating that SGRs belong to a young star population. Furthermore, two of these SGRs may be associated with clusters of very massive stars (Fuchs et al. 1999; Vrba et al. 2000; Eikenberry et al. 2001), strengthening the claim that these are young objects.

The burst repetition timescale for these sources varies from seconds to decades, while the bursts themselves are typically brief (durations ~ 0.1 s [e.g., Göğüş et al. 2001]). In contrast to these common brief bursts, two SGRs have each emitted one large long-duration burst. These large bursts, or "giant flares" as they are sometimes called, are distinguished by their extreme energies ($\sim 10^{44}$ ergs), their hard spectra at the onset, and their coherent pulsations during the decaying tail (lasting several minutes), reflecting the spin

of the underlying neutron star (Mazets et al. 1979; Hurley et al. 1999a; Feroci et al. 2001).

It is generally accepted today that SGRs are young, isolated, magnetized neutron stars. Both magnetic and gravitational (i.e., accretion) energy have been proposed as the source of the burst and persistent emission; however, the accretion models have difficulty explaining several properties of the burst emission (Thompson et al. 2000) as well as the lack of optical counterparts, particularly in the case of SGR 0526−66 (Kaplan et al. 2001). This source is located outside the Galactic plane and has a relatively small column density in its direction, while the other three confirmed sources all lie near the Galactic plane, where optical extinction is significant. A more convincing model is that the SGRs are magnetars, i.e., highly magnetized neutron stars ($B \sim 10^{14}$–10^{15} G) where magnetism is the largest source of free energy in the system (Duncan & Thompson 1992). In the magnetar model, the strong magnetic field of the neutron star powers the persistent emission through low-level seismic activity and heating of the stellar interior (Thompson & Duncan 1996) as well as the burst emission through large-scale crust fractures driven by an evolving magnetic field (Thompson & Duncan 1995). The super-Eddington burst fluxes are possible in the presence of such a strong field because of the suppression of electron scattering cross sections for some polarizations (Paczyński 1992).

In this paper we focus on SGR 1900+14, which has been the most prolific SGR in the last 3 yr. SGR 1900+14 is the source of one of the giant flares that was recorded on 1998 August 27 (Hurley et al. 1999a; Mazets et al. 1999; Feroci et al. 1999, 2001). Following the flare, the persistent X-ray flux of SGR 1900+14 increased dramatically and decayed over the next ~ 40 days as a power law in time with an index of ~ -0.7 (Woods et al. 2001). Nineteen days into the tail of this event, pointed X-ray observations revealed that the enhancement in flux was contained within the nonthermal component of the spectrum. In addition to this event, two other high-fluence events have shown extended X-ray tails directly following the burst. These two events were recorded on 1998 August 29 (Ibrahim et al. 2001) and more recently on 2001 April 18 (Guidorzi et al. 2001; Kouveliotou et al. 2001; Feroci et al. 2002; Woods et al. 2003).

[1] Calvin College, Department of Physics and Astronomy, Grand Rapids, MI 49546.

[2] Universities Space Research Association.

[3] NASA Marshall Space Flight Center, SD50, Huntsville, AL 35812.

[4] Hope College, Department of Physics and Engineering, Holland, MI 49422.

[5] University of California, Berkeley, Space Sciences Laboratory, Berkeley, CA 94720-7450.

[6] Ioffe Physical-Technical Institute, St. Petersburg 194021, Russia.

[7] NASA Goddard Space Flight Center, Greenbelt, MD 20771.

Here we present results on the spectral evolution and temporal decay of the X-ray tail of a burst recorded on 2001 April 28, 10 days after the intense April 18 event. Using data acquired with the *Rossi X-Ray Timing Explorer* (*RXTE*) Proportional Counter Array (PCA), we fit several spectral models to the tail flux to constrain the radiative mechanism that governs its emission. We further study in detail the evolution of the source pulse properties (pulse shape and fraction) during this decay and compare the energetics of all four events from SGR 1900+14 with extended tails. We discuss the implications of these results on the current models for SGR emissions.

2. 2001 APRIL 28 BURST

The reactivation of SGR 1900+14 on 2001 April 18 triggered a series of observations of the source with several satellites (*BeppoSAX*, *RXTE*/PCA, and *Chandra*). We observed the source with the *RXTE*/PCA several times during the subsequent 2 weeks and discovered an intriguing discontinuity in the source flux between consecutive *RXTE* orbits on April 28 (see Fig. 1). This trend was a strong indication of burst activity during Earth occultation of the source, since it was similar to the one observed during the 1998 August 29 event (Ibrahim et al. 2001), in which the decaying tail extended over multiple *RXTE* orbits. A search in *Ulysses* and *Wind*/Konus data revealed an intense burst on 2001 April 28, peaking approximately 121 s *before* our *RXTE* observations of the source resumed at a higher flux level. The Fourier spectra of the *RXTE* data provided an additional confirmation of the origin of the emission; the
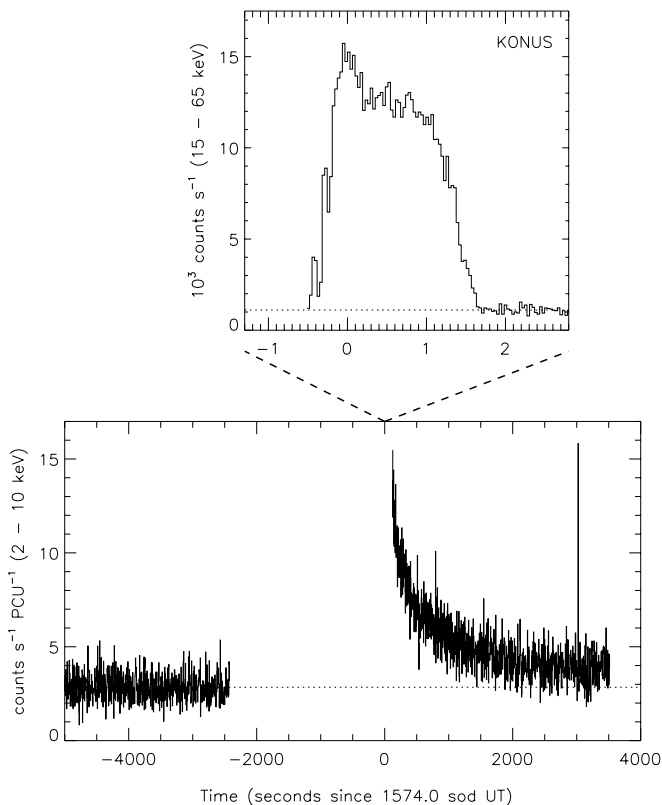

FIG. 1.—*Top:* Konus 25–100 keV time history of the 2001 April 28 burst from SGR 1900+14. The background level is indicated with a dotted line. *Bottom: RXTE*/PCA 2–40 keV light curve before and after the burst. The dotted line denotes the nominal background.

spin period of SGR 1900+14 is prevalent during the tail orbit but undetectable in the previous (quiescent) orbit.

2.1. *Gamma-Ray Observations*

On 2001 April 28, *Ulysses* and *Wind*/Konus observed a burst whose triangulated position (an annulus) contained SGR 1900+14. Its time history was unusual in that it had a duration of $\sim$2 s (Fig. 1), compared to the more common, short-duration SGR bursts. The Konus energy spectrum was well fitted by a power law times an exponential function [$dN/dE \propto E^{-0.5} \exp(-E/kT)$] with $kT = 21.2$ keV. We estimated the (25–100 keV) source fluence and peak flux (over 0.0625 s) to be 8.7×10^{-6} ergs cm^{-2} and 6.5×10^{-5} ergs cm^{-2} s^{-1}, respectively. The corresponding burst energy is $\sim$2.0 $\times 10^{41}$ ergs (assuming a source distance for SGR 1900+14 of 14 kpc; Vrba et al. 2000).

2.2. *X-Ray Observations*

2.3. *Spectral Analysis*

We removed all bursts, the Galactic ridge component, quiescent SGR flux, and other discrete X-ray sources for the spectral analysis of the X-ray tail emission as follows. We first subtracted the instrumental and *RXTE* orbital background from the source spectrum of the two orbits prior to the burst using PCABACKEST.[8] We then fitted the residual spectrum (2–30 keV), which is dominated by the Galactic ridge emission (Valinia & Marshall 1998), with a two-component function (power law plus Gaussian iron line). The width of the iron line was fixed at 0.4 keV, while the other parameters were allowed to vary in this fit. Using this model, we obtained a good fit to the data ($\chi^2_\nu = 1.17$ for 52 degrees of freedom [dof]; see Table 1 for fit parameters). Please note that this spectral fit is *not* entirely the quiescent spectrum of the SGR but is rather the sum of the SGR quiescent spectrum with the Galactic ridge and other discrete X-ray sources in the PCA field of view. This is a key point as we are interested in fitting the spectrum of the SGR tail emission and *not* the sum of the tail plus quiescent SGR flux.

For the spectral analysis of the burst X-ray tail, we used the PCABACKEST background together with the spectrum defined above as our "total background." More specifically, we defined a two-part model, where one component is the presumed tail spectrum and the second (fixed) part is the remaining background as defined above (see Tables 1 and 2 for a summary of fit parameters). We have fitted several spectral functions to the time-integrated burst tail (900 s from the time the *RXTE* data start; see Fig. 2): bremsstrahlung, power law, and blackbody (each with interstellar absorption) yielding χ^2 values of 71.15, 119.7, and 21.24, respectively (29 dof for each). Clearly, the simple blackbody is the best fit to the data (0.85 chance probability of measuring χ^2 this large). We measure a temperature $kT = 2.35(5)$ keV, a radius $r = 1.74(9)$ km (assuming a 14 kpc distance), and an effective hydrogen column density $N_H = 0.2(9) \times 10^{22}$ cm^{-2}. We attempted to fit two-component models (blackbody plus power law and bremsstrahlung plus power law) to the spectrum, but the bremsstrahlung plus power law failed to give a statistically acceptable fit to the data ($\chi^2_\nu = 2.7$) and the inclusion of the

[8] See http://heasarc.gsfc.nasa.gov/docs/xte/xtegof.html and links therein.

TABLE 1
PERSISTENT EMISSION PARAMETERS

Date	N_H (10^{22} cm^{-2})	α[a]	Emission Line[b]	Line Width[b]	χ^2/dof
2001 Apr 28..............	1.7 ± 0.9	1.95 ± 0.08	6.62 ± 0.08	0.4 (frozen)	60.6/52
1998 Aug 29	3.1 ± 0.4	2.72 ± 0.05	6.4 ± 0.3	0.4 (frozen)	58.1/70

[a] Power-law photon index.
[b] Gaussian line profile, modeling Galactic ridge.

power-law component in the blackbody plus power-law model was formally not required, as evidenced by an F-test (probability $= 0.915$).

To study the spectral evolution of the tail, we divided the data into eight intervals with nearly equal number of counts in each and fitted them with the model determined above. We find that the column density (N_H) does not vary significantly across the tail, while the temperature (kT) decreases monotonically. Forcing the column density to be the same in each interval results in an $N_H = 0.5(8) \times 10^{22}$ cm^{-2}. The $RXTE$/PCA has low sensitivity below 2 keV and therefore has difficulty measuring low column densities. Hence, we fixed the column density at the value ($N_H = 2.4 \times 10^{22}$ cm^{-3}) measured during *Chandra* observations (Kouveliotou et al. 2001) that bracketed our PCA observations. Both the temperature and normalization (i.e., emitting area) decrease modestly through the tail (Fig. 3).

Finally, we performed phase-resolved spectroscopy on the data during the tail. For the first ~ 900 s of the tail (minus bursts), we accumulated spectra for 10 phase bins by folding the data on the spin ephemeris of the star (Woods et al. 2003). The background subtraction was handled in the same manner as before. We performed a simultaneous fit to the 10 phase-binned spectra using the blackbody model, again holding the N_H fixed. We find a marginally significant (1.5×10^{-3} chance probability) variation in kT versus pulse phase (Fig. 4).

2.4. *Temporal Analysis*

Using the blackbody spectral fit defined above, we measured the flux in four energy bands (2–5, 5–10, 10–20, and 2–20 keV) to characterize the flux decay as well as to determine the total fluence contained in the extended tail emission. The errors in the flux are underestimated, since we

equate the relative error in the count rate to the relative error in the flux. We fitted a power law ($F \propto t^{-\alpha}$), a broken power law ($F \propto t^{-\alpha_1}$ for $t < t_b$ and $F \propto t^{-\alpha_2}$ for $t > t_b$), and a power law times exponential [$F \propto t^{-\alpha} \exp(-t/\tau)$]. In each case α is the power-law decay index and F is the flux. The fit parameter t_b in the broken power-law case is the time of the "break" in the flux decay. We found that with the exception of the 2–5 keV energy band (which was best fitted by a single power law), the decay was equally well fitted by either power law times exponential or broken power law. We show the power law times exponential fit in Figure 5 and the power-law index and exponential decay constant in Table 3 for each energy band. We find that the exponential decay constant decreases with energy and the power-law index steepens with energy, each indicative of spectral softening with time. Since the tail is still detectable at the end of our observations, we quote a lower limit of $\gtrsim 3.5$ ks for the tail duration. The power law times exponential function rapidly turns over after about 5 ks, so integrating over longer timescales does not contribute significantly to the fluence. We thus integrate the power law times exponential function over 5 ks and find the fluence to be 3.0×10^{-7} ergs cm^{-2} in the 2–20 keV tail and 2.1×10^{-7} ergs cm^{-2} in the 2–10 keV tail. The corresponding energies are 7.0×10^{39} and 4.9×10^{39} ergs in the 2–20 and 2–10 keV energy bands, respectively.

In addition to the temporal characteristics of the flux decay, we studied the pulse properties of SGR 1900+14 during the X-ray tail. The precise ephemeris was determined elsewhere (Woods et al. 2003) from the complete $RXTE$/PCA data taken during the 2001 April reactivation. We folded seven time intervals during the decaying burst tail as well as the two orbits prior to the burst for comparison, all using 2–10 keV data.

TABLE 2
SUMMARY OF SPECTRAL FITS

Model	N_H (10^{22} cm^{-2})	kT (keV)	R_{bb}[a] (km)	α[b]	χ^2/dof
2001 Apr 28					
Blackbody....................................	0.2 ± 0.9	2.35 ± 0.05	1.74 ± 0.09	. . .	21.2/29
Bremsstrahlung...........................	13 ± 1	10.7 ± 0.9	. . .	. . .	71.1/29
Power law	17 ± 1	. . .	. . .	2.26 ± 0.08	119.7/29
1998 Aug 29					
Blackbody + power law	10 ± 2	2.2 ± 0.2	1.2 ± 0.4	2.1 ± 0.2	30.7/35
Bremsstrahlung...........................	10.2 ± 0.6	12.9 ± 0.7	. . .	. . .	30.1/37
Power law	14.0 ± 0.8	. . .	. . .	2.16 ± 0.05	55.5/37

[a] Blackbody radius without general relativistic correction (assumes $d = 14$ kpc).
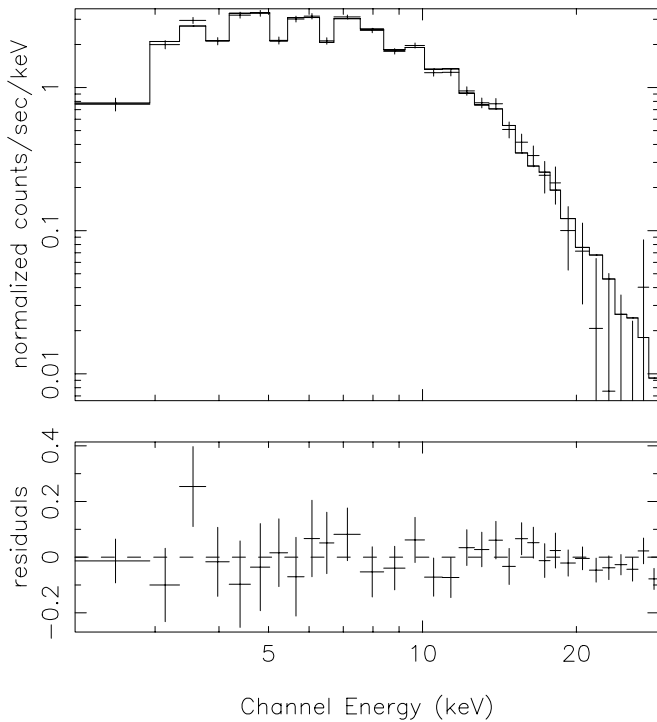[b] Power-law photon index.

FIG. 2.—900 s exposure of the 28 April 2001 *RXTE*/PCA spectrum with the attenuated (interstellar absorption) blackbody fit.
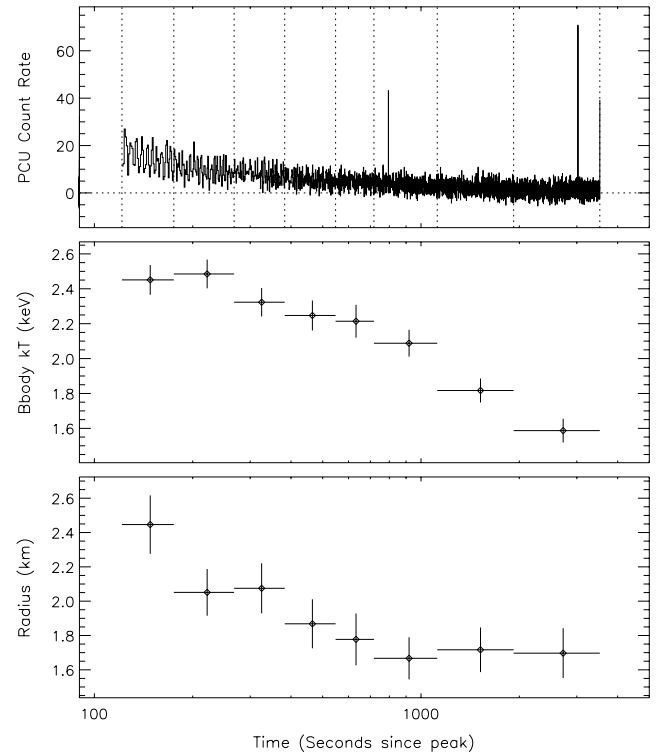

FIG. 3.—Parameters of the simple blackbody fit as a function of time for the 2001 April 28 decay. The top panel contains the light curve of the decay, the middle panel shows the blackbody temperature, and the bottom panel shows the radius of the emitting area. The vertical dotted lines in the top panel denote the time intervals over which spectra were fitted, and the horizontal dotted line is at zero counts s^{-1}. The radius was determined assuming a distance of 14 kpc to the source.

An accurate measure of the background level is required to measure the pulse fraction of the SGR during this epoch. Under normal circumstances, when the SGR is in quiescence, we cannot use the PCA data to determine the absolute level of the source flux because the contribution of the Galactic ridge is not well known and thereby introduces a systematic error in the absolute background determination that is comparable to the SGR count rate. However, the PCA cosmic background can be approximated during transient SGR flux enhancements (e.g., following strong bursts) under certain assumptions: (1) the PCA cosmic background is constant over this brief time interval, (2) PCA data *prior* to the flux increase are present, and (3) the pulse fraction of the SGR directly before the burst is known.

Chandra and *BeppoSAX* observations indicated that the level of the rms pulse fraction (2–10 keV) increased directly after the April 18 flare to ∼18% and subsequently decayed to ∼14% by May 1 (Kouveliotou et al. 2001; Woods et al. 2003). The pulse fraction is independent of energy in the 0.5–10 keV band during each of these epochs, and the pulse shape does not change significantly between epochs (Woods et al. 2003). From these data, we interpolated a pulse fraction of ∼14.3% for the pre–April 28 burst PCA data (i.e., the two orbits prior to the burst). We used this pulse fraction to determine the PCA cosmic background level during the preburst data on April 28 and assumed that this remains constant during the 0.2 day observation of the tail. Using the constant cosmic background level, we then measured the pulse fraction during the tail of the burst. The rms pulse fraction during the seven intervals of the tail and the inferred level (*dashed line*) are shown in Figure 6. We find that the pulse fraction increases significantly after the burst to ∼33%. For completeness, we performed the same analysis assuming the preburst pulse fraction was equal to the
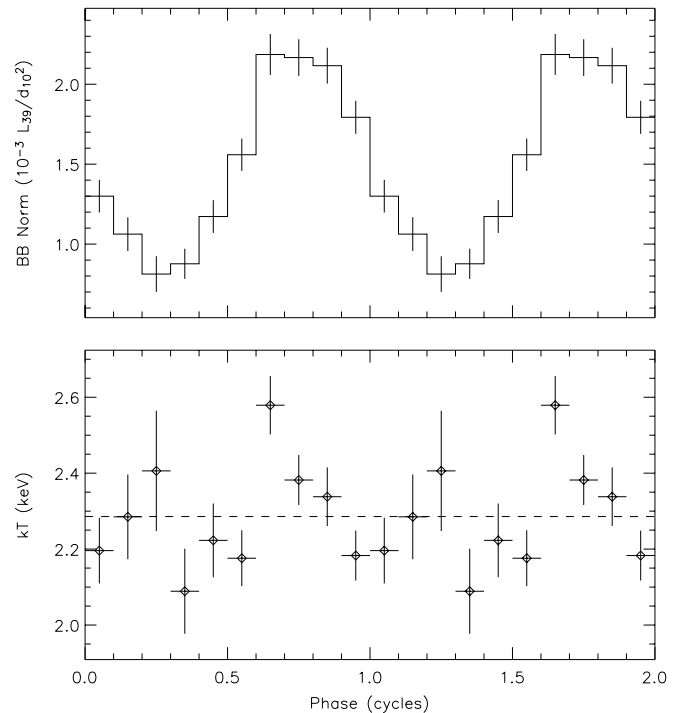
FIG. 4.—*Top:* Blackbody normalization as a function of phase for the 2001 April 28 decay. *Bottom:* Blackbody temperature as a function of phase for the 2001 April 28 decay.
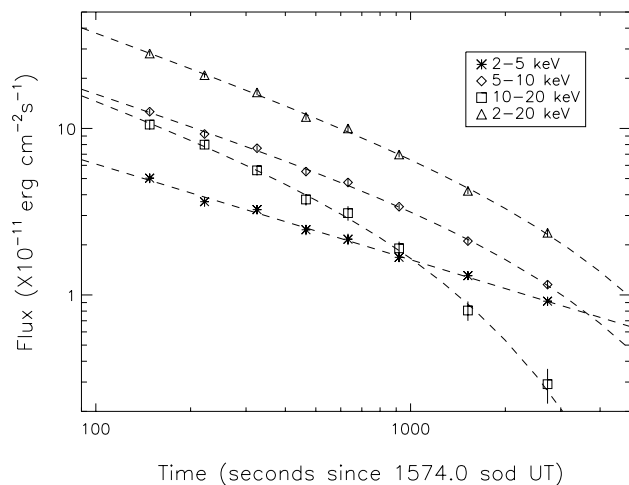
Fig. 5.—Temporal decay of the flux from the 2001 April 28 burst from SGR 1900+14 in three energy bands. The dashed lines are the best-fit power law times exponential function to each band.
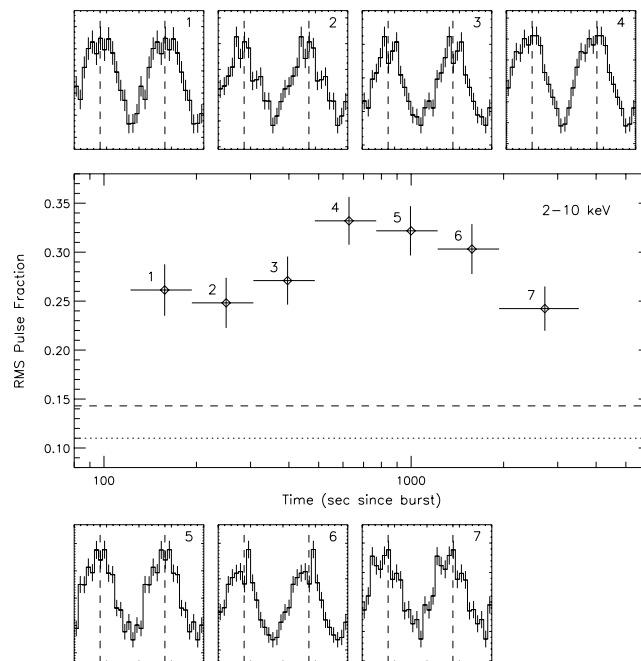

Fig. 6.—Pulsed fraction of SGR 1900+14 during the 2001 April 28 tail. The horizontal dashed line denotes the interpolated pulse fraction prior to the burst. The dotted line marks the nominal quiescent pulse fraction. The vertical dashed lines in the pulse profiles are the phase of pulse maximum. The pulse profiles shown cover two rotation cycles and have arbitrary flux units. The seven profiles correspond to the seven numbered data points in the middle panel.

nominal quiescent value of ~11% (Fig. 6, *dotted line*). This systematically lowers the measured pulse fractions by ~1.5% and thus does not change our results significantly.

We find no evidence for a systematic shift in phase of the pulse maximum or the slope of the phases (i.e., pulse frequency) relative to the predefined ephemeris, i.e., the pulse phase remained steady during the tail. Figure 6 exhibits the pulse profiles for seven intervals used in this analysis; we find that the shape is constant, with marginal changes (i.e., low-level phase noise).

Further, we investigated the phase occurrence of the burst itself. We first transformed the time history as observed with Konus to the solar system barycenter (SSB) using mission-specific tools. This transformation was confirmed by checking the alignment of an earlier burst observed from this source on 1998 August 29 recorded with Konus, the Burst and Transient Source Experiment (BATSE), and several other instruments (see § 3). We have used the BATSE time history for comparison because of its similar energy bandpass, good time resolution, and sensitivity. The BATSE time history of the August 29 burst was converted to the SSB using tools developed specifically for the BATSE mission (Wilson et al. 1993). A cross-correlation between the BATSE and Konus time histories shows that the relative transformation is accurate to within 14 ms for this event.

The absolute timing accuracy of Konus has been shown to be better than 5 ms through extensive testing within the Interplanetary Network. We will adopt 14 ms as our error in temporal precision (or 2.7×10^{-3} cycles in phase for SGR 1900+14) for the 2001 April 28 light curve.

The April 28 burst covers approximately 40% of the SGR 1900+14 pulse cycle (Fig. 7). The burst begins near pulse minimum and terminates at pulse maximum. The combined timing analysis results (pulse fraction, pulse shape, pulse phase, and burst phase) place significant constraints on the radiation mechanism during the tail (see § 4).

3. 1998 AUGUST 29 BURST

BATSE and *RXTE*/PCA observed another relatively intense event from SGR 1900+14 on 1998 August 29

TABLE 3
PARAMETERS OF FLUX DECAY

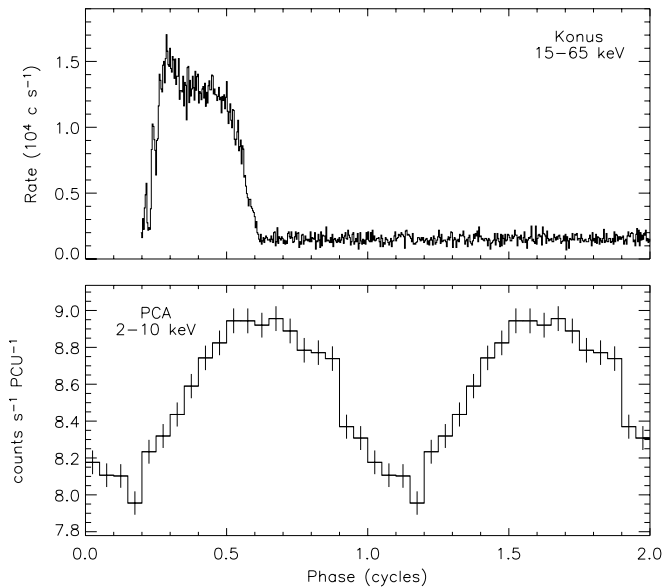| Event	Energy Band (keV)	Power-Law Index	Decay Constant (s)
2001 Apr 28..............	2–5	-0.58 ± 0.07	$> 8 \times 10^3$
	5–10	-0.62 ± 0.04	$4 \pm 1 \times 10^3$
	10–20	-0.7 ± 0.1	$1.5 \pm 0.4 \times 10^3$
	2–10	-0.62 ± 0.04	$8 \pm 2 \times 10^3$
	2–20	-0.68 ± 0.04	$5 \pm 1 \times 10^3$
1998 Aug 28	2–5	-0.43 ± 0.02	$5 \pm 1 \times 10^3$
	5–10	-0.43 ± 0.01	$2.6 \pm 0.2 \times 10^3$
	10–20	-0.57 ± 0.02	$1.21 \pm 0.09 \times 10^3$
	2–10	-0.43 ± 0.01	$3.5 \pm 0.4 \times 10^3$
	2–20	-0.510 ± 0.008	$2.9 \pm 0.2 \times 10^3$

FIG. 7.—Konus time history of the 2001 April 28 burst transformed to the solar system barycenter. The bottom panel shows the PCA pulse profile during the time interval surrounding the burst.

(Ibrahim et al. 2001). Similar to the 2001 April 28 event, it occurred in the days following a more energetic burst (on 1998 August 27) and exhibited a long duration X-ray tail. Unlike the April event, the August event had complete coverage with the *RXTE*/PCA (Fig. 8). To compare the tail characteristics for both events, we analyze below the August event using the same techniques that were implemented for the April event. We have defined the "tail" emission onset as the time where the bulk of the burst emission exhibits an abrupt decrease in flux ($\sim$3 s after $t = 0$ in Fig. 8). As discussed in Ibrahim et al. (2001), an abrupt change in the bremsstrahlung temperature is seen at the same time.

3.1. *Spectral Analysis*

We first quantified the PCA cosmic background (including $\sim$1000 s of preburst data. As in the April 28 tail, we find that a power law plus Gaussian iron line were sufficient to model the background spectrum. The width of the iron line was again fixed at 0.4 keV, while the rest of the parameters were allowed to vary in the fit (see Table 1). This model was removed from the data (i.e., added as a fixed model) for all subsequent spectral fitting of the August 29 X-ray tail.

For the August 29 event, we fitted bremsstrahlung, blackbody, power law, and blackbody plus power-law models, all having photoelectric absorption, to the entire first orbit of the tail spectrum. Consistent with the results of Ibrahim et al. (2001), only the bremsstrahlung and blackbody plus power-law models provided statistically acceptable fits to the data. In light of the April 28 tail results, we adopt the blackbody plus power-law model for this analysis. We measure a blackbody temperature $kT = 2.2(2)$ keV, a radius $r = 1.2(4)$ km (assuming a 14 kpc distance), a power-law photon index $\alpha = 2.1(2)$, and an effective hydrogen column density $N_H = 10(2) \times 10^{22}$ cm^{-2}.

Following the method of analysis in the April event, we divided the data into 11 segments with nearly equal counts, starting at the beginning of the tail. Since the
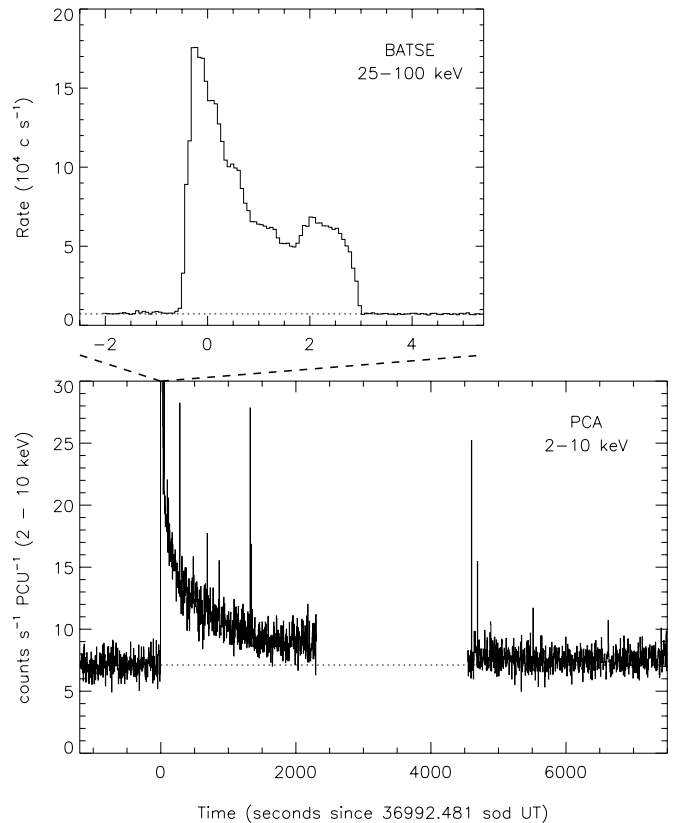

FIG. 8.—*Top: BATSE* light curve of the 1998 August 29 burst from SGR 1900+14. The background is denoted with the dotted line. *Bottom: RXTE*/ PCA light curve before and after the burst. The dotted line indicates the nominal background in both panels.

August event had complete coverage by the PCA, we were able to look at four additional intervals earlier in the tail. We simultaneously fitted all 11 intervals to a blackbody plus power-law fit and found the column density consistent with being constant. We also find that the photon power-law index is constant throughout the tail, and thus we force the column density and power-law index to be the same in each interval [$N_H = 10(2) \times 10^{22}$ cm^{-2} and $\alpha = 2.3(3)$, respectively]. The blackbody temperature shows a stronger decay than the April 28 event; however, the emitting area shows first a marginal decrease and then a slight rise to a larger final area than the beginning area (see Fig. 9). We note that the blackbody radius of the August 29 burst tail is mildly correlated with power-law spectral parameters in the fit, unlike the April 28 X-ray tail, where no power-law component was detected. Therefore, the modest evolution we observe in the radius may be an artifact of this cross-correlation, and these small changes could possibly be attributed to unmeasureable changes in the photon index. However, the observed changes in the blackbody temperature are too large to be accounted for from this effect. All of our spectral results on the August 29 burst tail are consistent with those found by Ibrahim et al. (2001).

3.2. *Temporal Analysis*

As in the April event, we used the best-fit spectrum to determine the flux in each time interval for four energy
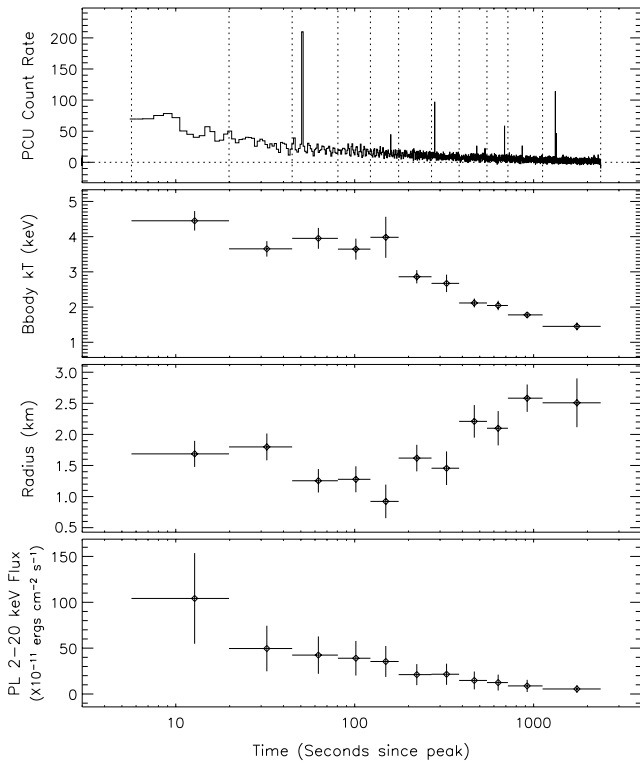
FIG. 9.—Parameters of the blackbody plus power-law fit as a function of time for the 1998 August 29 decay. The top panel contains the light curve of the decay, the second panel shows the blackbody temperature, the third panel shows the radius of the emitting area, and the bottom panel shows the flux of the power-law component. The vertical dotted lines in the top panel denote the time intervals over which spectra were fitted, and the horizontal dotted line is at zero counts s^{-1}. The radius was determined assuming a distance of 14 kpc to the source.
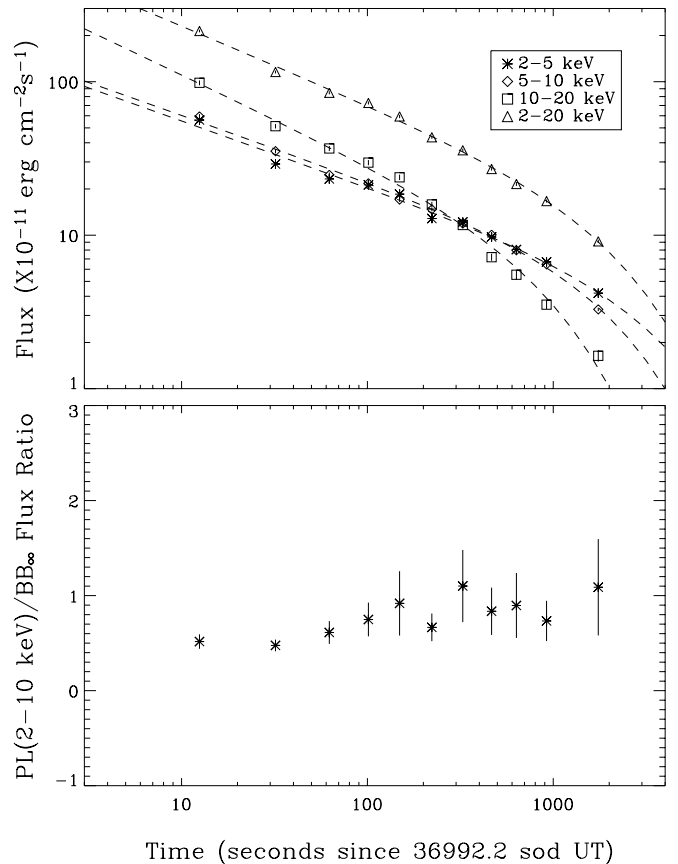

FIG. 10.—Top panel shows temporal decay of the flux from the 1998 August 29 burst from SGR 1900+14 in three energy bands. The dashed lines indicate the best-fit power law times exponential function in each energy band. The bottom panel shows the ratio of the power-law flux in the 2–10 keV energy band to bolometric blackbody flux.

bands (2–5, 5–10, 10–20, and 2–20 keV). Again, the errors in the flux are underestimated, since we equate the relative error in the count rate to the relative error in the flux. We find that for all energy bands the decay is best fitted equally well by the broken power law and power law times exponential. We show in Figure 10 the power law times exponential fit for each energy band with fit parameters given in Table 3. We also show in Figure 10, the ratio of the power-law flux in the 2–10 keV energy band to bolometric blackbody flux. The ratio shows that at early times the blackbody component dominates, while at later times the ratio increases to around 1, consistent with the results of Marsden & White (2001). Similar to the April 28 event, the exponential decay constant decreases with energy and the power-law index steepens with energy, indicating spectral softening with time.

In the *RXTE* orbit directly following the August burst, the SGR count rate (2–10 keV) remained significantly higher ($>5\,\sigma$) than the measured preburst background. During the subsequent orbit, the count rate was consistent with the preburst background; thus we estimate the duration of this tail to be ~ 8 ks, or the end of the last orbit in which the tail was detected. Integrating the fit over 8 ks yields a fluence and energy in the 2–20 keV tail of 6.4×10^{-7} ergs cm^{-2} and 1.4×10^{40} ergs, respectively, and in the 2–10 keV tail of 4.8×10^{-7} ergs cm^{-2} and 1.1×10^{40} ergs, respectively.

We then measured the pulse fraction for the August 29 event using the same technique as before. Unfortunately, we

do not have pulse fraction measurements closely bracketing this event; the closest reliable rms pulse fraction was measured with *BeppoSAX* at 12% on 1998 September 15–16 (2–10 keV). Using this value as the " background," we find for eight intervals during the tail that the pulse fraction increased to a maximum of $\sim 20\%$ at ~ 200 s after the burst peak and returned to the preburst value after several thousand seconds (Fig. 11). If we vary the assumed preburst pulse fraction to 8% and 16%, the resulting maximum pulse fraction values measured during the tail change to $\sim 17\%$ and $\sim 22\%$, respectively. Independent of the assumed value of the preburst pulse fraction, the increase of the pulse fraction from preburst to postburst remains highly significant.

Pulse shape changes are more prevalent during the tail of this event. We note that the centroid of the primary peak is shifted in phase and the width of the pulse broadens relative to the preburst pulse profile during the first ~ 30 s. After the first 30 s, the phase and shape of the profile returns to the preburst profile as the pulse fraction rises. Thereafter, the phase of the average profile remains steady, although some low-level noise in the shape of the profile persists.

We next investigated the phase occurrence of the August 29 burst. The time history of the August 29 burst as observed with BATSE was transformed to the SSB and converted to pulse phase for SGR 1900+14 according to the spin ephemeris found from previous work (Woods et al. 1999b). The BATSE light curve and PCA (2–10 keV) folded
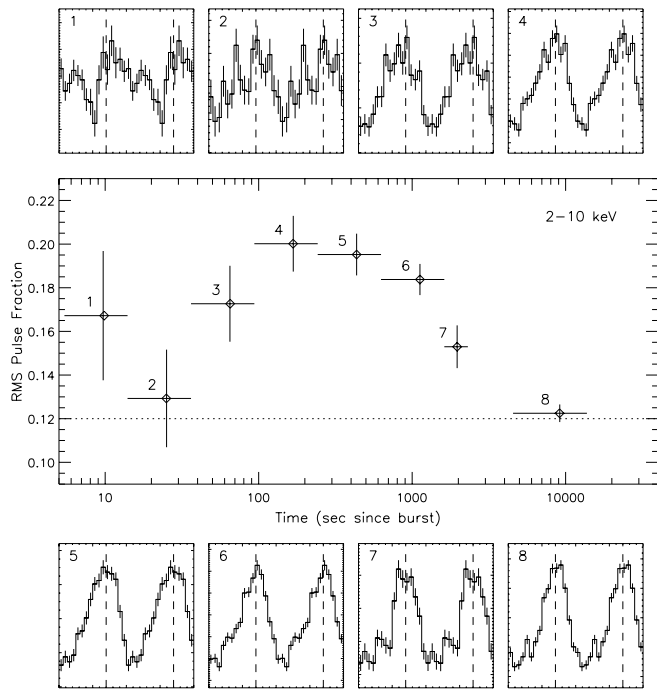
FIG. 11.—Pulsed fraction in the 1998 August 29 decay. The horizontal dotted line indicates the pulse fraction prior to the burst. The vertical dashed lines in the pulse profiles are the phase of pulse maximum. The eight profiles correspond to the eight numbered data points in the middle panel.

pulse profile from August 29 (minus bursts) are shown in Figure 12. The burst peak at gamma-ray energies lags slightly behind the centroid of the X-ray pulse maximum ($\sim$0.1 cycle), although the onset of the primary burst emission coincides with pulse maximum to within the errors.
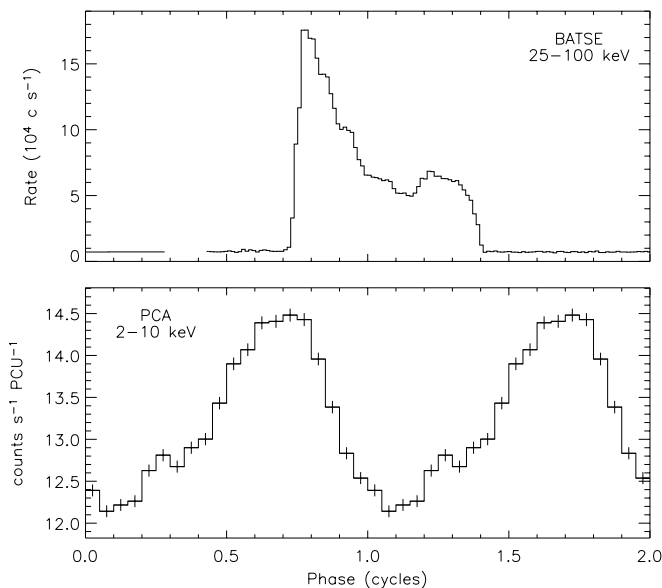

FIG. 12.—BATSE time history of the 1998 August 29 burst transformed to the solar system barycenter. The bottom panel shows the pulse profile during the time interval surrounding the burst.

4. BURST COMPARISON

The 1998 August 29 and 2001 April 28 bursts occur under very similar conditions and originate at the same source, SGR 1900+14. They both occur within days of much larger bursts or flares (1998 August 27 and 2001 April 18). We therefore searched for similarities in temporal, spectral, and pulse properties between these two events. We have shown that the X-ray tails in both cases demonstrate spectral softening as the flux decays. The rms pulse fraction in both events was shown to rise by about a factor $\sim$2–3 during the tails of each event, while the phase of the pulsations remained more or less steady. Finally, the bursts themselves cover separate regions of pulse phase. The start times of these two bursts in gamma rays are $\sim$180° out of phase from one another.

Since the August 29 event showed clear evidence of a power-law component, we investigated whether the absence of the power-law component in the April 28 burst tail was due to lack of sensitivity or a significantly reduced relative contribution from a hypothetical power-law component. If the April 28 burst tail contained the same relative contribution of power law to total flux as the August 29 burst, then the expected power-law flux in the time integrated 2–20 keV April 28 tail would be 1.5×10^{-10} ergs cm^{-2} s^{-1}. We proceeded to fit the time integrated April 28 burst tail to a blackbody plus power-law model. All parameters were allowed to vary except the power-law photon index, which was fixed at the best-fit value for the August 29 burst tail ($\alpha = 2.1$). Fixing the photon index was required to obtain convergence in the fit. As expected, the power-law flux was consistent with zero having an upper limit of 8.0×10^{-11} ergs cm^{-2} s^{-1} (90% confidence), a factor of 2 lower than the expected flux. We conclude that the April 28 burst tail is exclusively thermal and intrinsically different than the August 29 burst tail.

We have estimated the energies in the tails of both the 2001 April 28 burst and 1998 August 29 burst in the previous sections. We find that the ratio of energy output in the tail versus burst energy are very similar for these two bursts (0.024 and 0.025, respectively). In Table 4 we include energy estimates of the X-ray tails following the 2001 April 18 (Feroci et al. 2003) and the 1998 August 27 flares from SGR 1900+14 as well and find similar tail to burst energy output ratios. For the April 18 flare, we have assumed the power-law fit to the X-ray tail plus persistent emission when calculating the tail energy. Because of the poor temporal coverage for this event and the presence of a bump in the tail decay, the tail energy of this event is poorly determined (M. Feroci 2003, in preparation).

For the August 27 flare, the X-ray tail remains above the nominal persistent emission level for $\sim$40 days (Woods et al. 2001). Unfortunately, the coverage of this tail is not as

TABLE 4
BURST FLUENCES (25–100 keV) AND TAIL FLUENCES (2–10 keV)

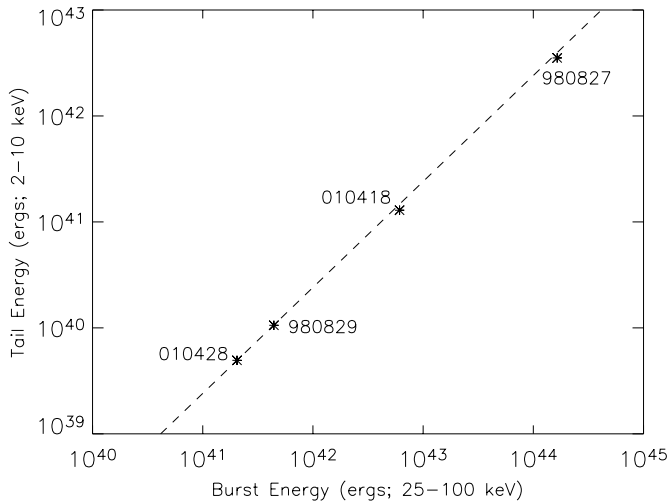| Event	Tail Fluence (ergs cm^{-2})	Burst Fluence (ergs cm^{-2})
1998 Aug 27	1.5×10^{-4}	7.0×10^{-3}
1998 Aug 29	4.8×10^{-7}	1.9×10^{-5}
2001 Apr 18.........................	5.5×10^{-6}	2.6×10^{-4}
2001 Apr 28.........................	2.1×10^{-7}	8.7×10^{-6}

Fig. 13.—Tail energy vs. burst energy output of four separate bursts from SGR 1900+14. An assumed distance of 14 kpc is used.

complete as it is for the August 29 and April 28 bursts. Therefore, in order to estimate the tail energy from the limited information available, we must assume that the 2–10 keV spectrum and pulse fraction remain constant throughout the decay of the tail. Each of these assumptions is consistent with the published work on this X-ray tail. The 2–10 keV pulse fraction measured at 19 days into this tail was found to be consistent with the quiescent pulse fraction of ∼11% (Woods et al. 2001). Furthermore, the 2–5/5–10 keV pulsed amplitude softness ratio of SGR 1900+14 (a coarse measurement of the spectrum within 2–10 keV) during this tail was found to show only modest (∼25%) variations (Göğüş et al. 2002). To estimate the X-ray energy in the tail of the August 27 flare, we integrated a power-law fit to the pulsed flux measurements in the 2–10 keV band (Woods et al. 2001) between the end of the burst as observed in gamma rays (Feroci et al. 2001) and 40 days following the flare minus the persistent emission flux over the same time interval. We measure a tail fluence of 1.5×10^{-4} ergs cm^{-2} or an isotropic energy of $3.5 \times 10^{42} d_{14\,\mathrm{kpc}}^2$ ergs.

The burst and tail energies of the four tails are plotted in Figure 13. The data agree remarkably well with a constant tail to burst energy fraction (i.e., are consistent with the dotted line, which has a fixed slope of unity). The average ratio of tail to burst energy for these four bursts from SGR 1900+14 is ∼2%. Note that this fraction reflects the ratio over finite, yet consistent energy bands.

5. DISCUSSION

We have detected, for the first time, a cooling, exclusively thermal X-ray tail following a burst from SGR 1900+14 recorded on 2001 April 28. During the first ∼1 ks of the X-ray tail, we measure a 35% decrease in the blackbody temperature and a 30% reduction in the emitting area. At all times, the inferred emitting area encompasses a small fraction of the neutron star surface, assuming a 10 km radius neutron star. We have confirmed earlier work (Ibrahim et al. 2001) that showed a strong cooling blackbody present in the August 29 burst tail. These observations of enhanced thermal emission during burst tails provide strong evidence for burst-induced surface heating in SGR 1900+14.

The pulse properties of these tails further constrain the location of the heating on the stellar surface following the bursts. In quiescence, SGR 1900+14 has a pulse fraction of 11%. In order to increase the pulse fraction without changing the shape or phase of the pulse profile, one requires that the additional emission that increases the pulse fraction come from the same region of the stellar surface that is responsible for the peak of the quiescent pulsations. For the sake of argument, we will assume this region to be the polar cap. For example, suppose a region of the stellar surface were heated and its location was at the same magnetic longitude but different latitude than the polar cap. For small offsets in latitude angle, this scenario could account for a similar pulse profile, constancy of the pulse phase from pre-burst to postburst and, depending upon the observer's geometry, an increase in pulse fraction. For large offsets, all three observables will be altered in a manner opposite to what is observed. Alternatively, one could have a small hot spot emerge at a different longitude but the same latitude. For small offsets in longitude angle this is compatible with observations. However, large offsets in longitude will present a phase lag (or lead) in the pulse maximum, a change in pulse profile, and a decrease in pulse fraction. Considering these two scenarios, we conclude that the observations restrict the region of enhanced emission to be located within an ellipse surrounding the polar cap. Note that there are no stringent constraints on the altitude of the excess emission, only the angular position relative to the magnetic axis. Quantifying the restrictions in magnetic longitude and latitude is difficult as it will depend upon the observer's geometry, gravitational light bending, beam geometry, and so on.

We have shown that the August 29 and April 28 events began approximately 180° apart in phase. Earlier work by Palmer (2000) showed that the occurrence in phase of bursts from SGR 1900+14 during late August and early 1998 September were random. This was true for all bursts as well as subsets of bursts at different energies. The random occurrence of bursts in pulse phase indicates that the bursts themselves are not localized near the region contributing to the pulsed emission; however, the ensuing flux enhancements (well correlated with burst activity [Woods et al. 2001]) indicate localized heating near the putative polar cap.

With these observational constraints in mind, we now consider the magnetar model. In this model, it is postulated that the build up of magnetic stresses within the neutron star crust are sufficient to overcome the tensile strength of the crust and crack it (Thompson & Duncan 1995). Fracturing the stellar crust perturbs field lines and ultimately leads to a trapped pair-photon fireball. Thompson & Duncan (1995) considered the likelihood of heating of the neutron star surface by the resultant trapped fireball suspended above the fracture site. For shallow heating, they estimated the cooling timescale to be equivalent to the burst duration. In this timescale estimate, however, they did not account for the possibility of vertical expansion against gravity in the atmosphere, which could extend passive surface cooling up to ∼10³ s (Lynbarsky, Eichler, & Thompson 2002). Thompson et al. (2002) also showed that longer timescale cooling can also be achieved through deep heating of the crust that leads to a longer conduction time of the heat to the surface and that the temporal evolution of cooling after deep crustal heating could resemble a power law in time with a decay index of ∼−0.7. This picture fits nicely with the cooling thermal components observed during these X-ray tails.

One requirement of this model with regard to these data is that the burst fracture site be located at or very near one of the magnetic poles. The proximity of the fracture site (i.e., burst) to the polar cap vicinity is required to satisfy the constraints introduced by the pulsed flux observations. For this model to work, however, the bursts themselves must be visible at all rotational phases (i.e., even when the polar cap is facing opposite the observer). This suggests that the light emitted from the burst originate at sufficiently high altitudes or must be scattered, as has been suggested for the persistent emission from these sources (Thompson et al. 2002). However, the trapped fireball for most bursts is held close to the surface, and it is questionable whether strong scattering can occur at much higher luminosities than the persistent X-ray luminosity and for higher photon energies, particularly without substantial spectral variations in the bursts with pulse phase.

An alternative to explain these observations would be that the bursts have a magnetospheric origin (Lyutikov 2002). Here we consider a concentric sphere surrounding the neutron star at a large radius ($R > 10R_*$) where magnetic reconnection is occurring and giving rise to SGR bursts. The high altitude allows bursts to be observed for nearly all rotational phases. Moreover, the field lines permeating this surface are preferentially concentrated at the magnetic poles. Hence, particles accelerated along these field lines will impact the stellar surface at the polar cap regions. This scenario we have outlined is qualitatively compatible with the observations, although further quantitative modeling is needed with regard to surface heating/cooling by ablation, burst timescales, burst spectra, etc., before it can be considered further.

Finally, the observation that the ratio of tail to burst energy is consistent with being constant between the four events from SGR 1900+14 is an intriguing one. However, we would like to stress that this result is based upon a small number of events and some using predominantly inferred fluxes from the measured pulsed intensity; therefore, we regard this currently as a tentative result. In addition to potentially confirming this result, the detection of several more SGR burst tails will provide useful diagnostics for the burst mechanism, as shown by this work. Assuming that the observed conversion of burst to tail energy extends to lower energy burst events, X-ray tails can be observed from the more plentiful low-energy SGR bursts (down to $\sim 2 \times 10^{39} d^2_{14\,\mathrm{kpc}}$ ergs) with sensitive, low-background X-ray telescopes such as *Chandra* and *XMM-Newton*.

REFERENCES

Duncan, R., & Thompson, C. 1992, ApJ, 392, L9
Eikenberry, S. S., et al. 2001, ApJ, 563, L133
Feroci, M., Frontera, F., Costa, E., Amati, L., Tavani, M., Rapisarda, M., & Orlandini, M. 1999, ApJ, 515, L9
Feroci, M., Hurley, K., Duncan, R. C., & Thompson, C. 2001, ApJ, 549, 1021
Fuchs, Y., Mirabel, F., Chaty, S., Claret, A., Cesarsky, C. J., & Cesarsky, D.A. 1999, A&A, 350, 891
Göğüş, E., Kouveliotou, C., Woods, P. M., Thompson, C., Duncan, R.C., & Briggs, M. S. 2001, ApJ, 558, 228
Göğüş, E., et al. 2002, ApJ, ApJ, 577, 929
Guidorzi, C., et al. 2001, GCN Circ. 1041
Hurley, K. 2000, in AIP Conf. Proc. 526, Gamma-Ray Bursts: 5th Huntsville Symp., ed. R. M. Kippen, R. S. Mallozzi, & G. J. Fishman (New York: AIP), 763
Hurley, K., et al. 1999a, Nature, 397, 41
———. 1999b, ApJ, 510, L111
Ibrahim, A., Strohmayer, T. E., Woods, P. M., Kouveliotou, C., Thompson, C., Duncan, R. C., Dieters, S., van Paradijs, J., & Finger M. 2001, ApJ, 558, 237
Kaplan, D. L., Kulkarni, S. R., van Kerkwijk, M. H., Rothschild, R. E., Lingenfelter, R. L., Marsden, D., Danner, R., & Murakami, T. 2001, ApJ, 556, 399
Kouveliotou, C., et al. 1998, Nature, 393, 235
———. 1999, ApJ, 510, L115
———. 2001, ApJ, 558, L47

Lynbarsky, Y., Eichler, D., & Thompson, C. 2002, ApJ, 580, L69
Lyutikov., M. 2002, ApJ, 580, L65
Marsden, D., & White, N. E. 2001, ApJ, 551, L155
Mazets, E. P., Cline, T., Aptekar, R. L., Butterworth, P., Frederiks, D. D., Golenetskii, S. V., Il'inskii, V. N., & Pal'shin, V. D. 1999, Astron. Lett., 25, 635
Mazets, E. P., et al. 1979, Nature, 282, 587
Paczyński, B. 1992, Acta Astron., 42, 145
Palmer, D. M. 2001, Mem. Soc. Astron. Italiana, 73, 578
Thompson, C., & Duncan, R. 1995, MNRAS, 275, 255
———. 1996, ApJ, 473, 322
Thompson, C., Duncan, R., Woods, P. M., Kouveliotou, C., Finger, M. H., & van Paradijs, J. 2000, ApJ, 543, 340
Thompson, C., Lyutikov, M., & Kulkarni S. R. 2002, ApJ, 574, 332
Valinia, A., & Marshall, F. E. 1998, ApJ, 505, 134
Vrba, F. J., Henden, A. A., Luginbuhl, C. B., Guetter, H. H., Hartmann, D. H., & Klose, S. 2000, ApJ, 533, L17
Wilson, R. B., et al., in Proc. Los Alamos Workshop, ed. K.A. Van Riper, R. Epstein, & C. Ho (New York: Cambridge Univ. Press), 257
Woods, P. M., Kouveliotou, C., Göğüş, E., Finger, M. H., Swank, J., Smith, D. A., Hurley, K., & Thompson, C. 2001, ApJ, 552, 748
Woods, P. M., Kouveliotou, C., van Paradijs, J., Finger, M. H., & Thompson, C. 1999a, ApJ, 518, L103
Woods, P. M., et al. 1999b, ApJ, 524, L55
———. 2003, ApJL, submitted